ChemPubSoc Europe

DOI: 10.1002/cssc.201600679

CHEMSUSCHEM Communications

Effect of Halide Composition on the Photochemical Stability of Perovskite Photovoltaic Materials

Ravi K. Misra[+],[a, b] Laura Ciammaruchi[+],[a] Sigalit Aharon,[b] Dmitry Mogilyansky,[c] Lioz Etgar,[b] Iris Visoly-Fisher,*[a, c] and Eugene A. Katz*[a, c]

The photochemical stability of encapsulated films of mixed halide perovskites with a range of $MAPb(I_{1-x}Br_x)_3$ (MA = methylammonium) compositions (solid solutions) was investigated under accelerated stressing using concentrated sunlight. The relevance of accelerated testing to standard operational conditions of solar cells was confirmed by comparison to degradation experiments under outdoor sunlight exposure. We found that $MAPbBr_3$ films exhibited no degradation, while $MAPbI_3$ and mixed halide $MAPb(I_{1-x}Br_x)_3$ films decomposed yielding crystallization of inorganic PbI_2 accompanied by degradation of the perovskite solar light absorption, with faster absorption degradation in mixed halide films. The crystal coherence length was found to correlate with the stability of the films. We postulate that the introduction of Br into the mixed halide solid solution stressed its structure and induced more structural defects and/or grain boundaries compared to pure halide perovskites, which might be responsible for the accelerated degradation. Hence, the cause for accelerated degradation may be the increased defect density rather than the chemical composition of the perovskite materials.

[a] Dr. R. K. Misra,[+] Dr. L. Ciammaruchi,[+] Dr. I. Visoly-Fisher, Prof. E. A. Katz
Dept. of Solar Energy and Environmental Physics
Swiss Institute for Dryland Environmental and Energy Research
The Jacob Blaustein Institutes for Desert Research (BIDR)
Ben-Gurion University of the Negev
Midreshet Sede Boqer 8499000 (Israel)
E-mail: irisvf@bgu.ac.il
keugene@bgu.ac.il

[b] Dr. R. K. Misra,[+] S. Aharon, Dr. L. Etgar
Casali Center for Applied Chemistry
The Institute of Chemistry
The Hebrew University of Jerusalem
Jerusalem 9190401 (Israel)

[c] Dr. D. Mogilyansky, Dr. I. Visoly-Fisher, Prof. E. A. Katz
Ilse Katz Institute for Nanoscale Science & Technology
Ben-Gurion University of the Negev
Be'er Sheva 8410501 (Israel)

[+] These authors contributed equally to this work.

Supporting Information for this article can be found under: http://dx.doi.org/10.1002/cssc.201600679. It includes a schematic representation of the solar concentrator, UV/Vis absorption spectra for the mixed halide $MAPb(I_{1-x}Br_x)_3$ perovskite films, $PbBr_2$ absorbance spectrum, FTIR spectra of the $MAPbI_3$ film before and after exposure, SEM images, diffuse reflectance spectra, and the calculation method of the number of absorbed solar photons.

This publication is part of a Special Issue focusing on the "Stability of Perovskite Solar Cells & Devices". A link to the issue's Table of Contents will appear here once it is complete.

Organic–inorganic hybrid perovskites have recently achieved a breakthrough in the field of thin film photovoltaics (PV), with extremely high power conversion efficiencies (PCE) of over 20% for wet-processed devices.[1] The structure of such perovskites is AMX_3, where M is a divalent metal cation, X are halides, and A is an organic cation. Such perovskites have excellent properties for PV sunlight conversion, including direct band gaps, large absorption coefficients, and high carrier mobility.[2] The ability to tune the energy band gap by changing the halide anion composition is another important advantage of these materials.[3] Noh et al. showed colorful, efficient perovskite solar cells using different I/Br ratios with PCEs of up to 12.3%.[4] Aharon et al. used a two-step deposition technique to synthesize $MAPb(I_{1-x}Br_x)_3$ (MA = methylammonium; $0 \le x \le 1$) perovskites and utilized them in hole-conductor-free PV cells that combined the good perovskite hole conduction and tunable absorption spectrum.[5]

A significant challenge en route to commercialization of perovskite-based PV is the development of devices combining high PCE and operational stability. Accelerated stability tests[6] can rapidly screen different PV materials and enhance the development of stable and efficient devices. Recently we demonstrated such an accelerated stability study of perovskite thin films using concentrated sunlight.[7] In particular, encapsulated $MAPbBr_3$ films were shown to be more stable than $MAPbI_3$ films following exposure to concentrated sunlight of 100 suns (1 sun = 100 mW cm^{-2}), with the latter decomposing into PbI_2 and organic components under light combined with elevated temperatures. We then postulated that combining the better photovoltaic performance of $MAPbI_3$ with the added stability of its bromide counterpart, by using mixed compositions of $MAPb(I_{1-x}Br_x)_3$, would yield an optimized PV material.[7] Noh et al. demonstrated enhanced "shelf-life" stability of the PCE of cells based on $MAPb(I_{1-x}Br_x)_3$ with x ranging between 0.2 and 0.29, after cell storage in the dark in controlled humidity atmosphere.[4] Rong et al., in their review article, attributed this improved stability to the more compact and dense crystal structure of the mixed halide perovskites.[8] On a different note, reversible instability phenomena were demonstrated in relatively Br-rich compositions: Hoke et al.[9] noted a change in photoluminescence (PL) in films with $x \ge 0.2$ under visible light soaking, which was attributed to segregation into iodide-rich and bromide-rich domains. This change was fully reversible after few minutes in the dark, hence it cannot be related to long-term degradation. Sadhanala et al. noticed the possible existence of two phases in fresh mixed halide films with $x = 0.4$ and 0.6, which evolved into a single phase after a few days of

storage at room temperature, with no further changes.[10] Though both phenomena were short-termed, they may point to certain instability of mixed halide films at specific compositions.

Stability of PV perovskite materials can be studied with respect to the storage stability (i.e., shelf life) in the dark and at different environments, or with respect to the operational stability of encapsulated samples under solar illumination. Towards focusing on the latter, herein we compare the photochemical stability of encapsulated films of mixed halide perovskites with a range of $MAPb(I_{1-x}Br_x)_3$ compositions under accelerated stressing tests using concentrated natural sunlight at 100 suns. The results are compared to degradation under outdoor sunlight exposure to establish the relevance of the accelerated testing to standard operational conditions of PV cells. The evolution of light absorption and the corresponding structural modifications in the films following stressing were investigated. Contrary to our initial presumption, we found that $MAPbI_3$ and $MAPbBr_3$ were more stable than mixed halide compositions, under both concentrated and standard solar exposures. The reasons for the reduced stability of the mixed halide compositions are discussed below. Understanding the perovskite material stability can be used towards understanding cell stability, where other failure mechanisms may also be involved.

The film structure and composition were studied using UV/Vis absorbance spectroscopy and X-ray diffraction (XRD). Figure 1 and 2 show the XRD patterns of $MAPb(I_{1-x}Br_x)_3$ films of various compositions, and their properties are summarized in Table 1. XRD patterns of $MAPbI_3$ and $MAPbBr_3$ films for the entire 2θ ranges (Figure 1, plots 1 and 5) indicate their tetragonal *I*4/*mcm* and *Pm*$\bar{3}$*m* cubic perovskite structures, respectively.[4,11] For pure $MAPbI_3$ (bottom curve in Figure 2), two diffraction peaks located at 28.11° and 28.36° are associated with the (004) and (220) planes in the tetragonal *I*4/*mcm* phase.[12] In accordance with a recent report,[4] increasing *x* was found to result in: (a) a pattern shift to larger scattering angles (Figure 2) and the corresponding decrease of the lattice parameters (Table 1), and (b) merging of the (004) and (220) peaks to a single peak at 28.5°. Finally, the XRD pattern of the pure $MAPbBr_3$ (upper curve in Figure 2) exhibited a narrow peak at 30.1°, associated with the (200) plane in the *Pm*$\bar{3}$*m* cubic phase.

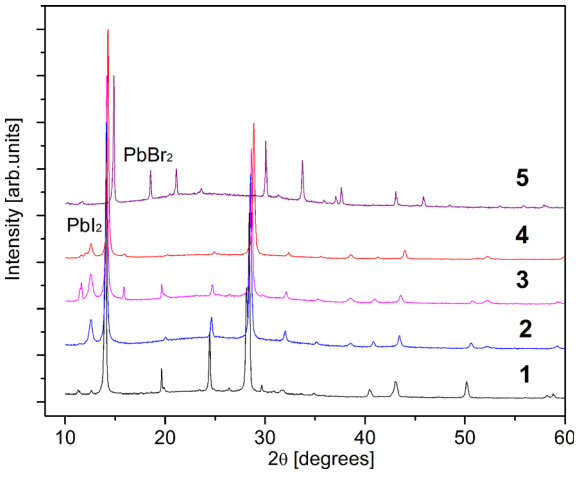

Figure 1. XRD patterns of as-produced $MAPb(I_{1-x}Br_x)_3$ films. Increasing sample numbers indicate increasing Br content; for sample details see Table 1.

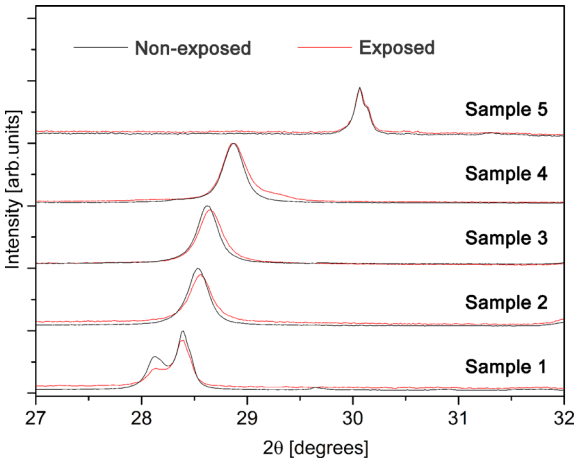

Figure 2. XRD patterns of $MAPb(I_{1-x}Br_x)_3$ thin-films in the 2θ range between 27–32° before and after exposure to concentrated sunlight of 100 suns for 1 h. Increasing sample numbers indicate increasing Br content; for sample details see Table 1.

Table 1. The halide compositions and structural parameters of $MAPb(I_{1-x}Br_x)_3$ thin films.

Sample	MAI/MABr[a]	Lattice parameter [Å]	FWHM[b] [°]	Br content, *x* expected[c]	calculated[d]	E_g[e] [eV]
1	1:0	6.312[f]	0.16	0	0	1.55
2	2:1	6.256	0.228	0.11	0.15 ± 0.02	1.65
3	1:1	6.236	0.223	0.16	0.20 ± 0.03	1.69
4	1:2	6.186	0.226	0.22	0.33 ± 0.03	1.78
5	0:1	5.934	0.1	1	1	2.31

[a] Ratio in the organic precursor solution. [b] The peaks' full width at half maximum (FWHM) was determined for the (200) peak of the cubic lattice or averaged for (004) and (220) peaks of the tetragonal lattice (see Figure 2). [c] According to the precursor materials. [d] Calculated from the XRD data assuming Vegard's law. [e] The optical bandgap, determined from UV/Vis spectrum. [f] The parameter was calculated for pseudo-cubic (*pc*) lattice.[4]

The actual halide composition of the films was determined and compared to that in the precursor solutions. According to Vegard's law, the variation of the lattice parameter in a homogeneous alloy (solid solution) is linear with composition.[13] Noh et al.[4] suggested the relevance of this rule for their $MAPb(I_{1-x}Br_x)_3$ films at the entire range of x ($0 \leq x \leq 1$). Applying Vegard's law to our XRD results showed a small difference in the Br content between the expected and actual composition (Table 1). Recently, Fedeli et al.[14] demonstrated a small negative deviation from Vegard's law for $x \geq 0.19$ in $MAPb(I_{1-x}Br_x)_3$ films, which they referred to the shift from tetragonal to cubic crystal structure. In our case, we believe that such a deviation

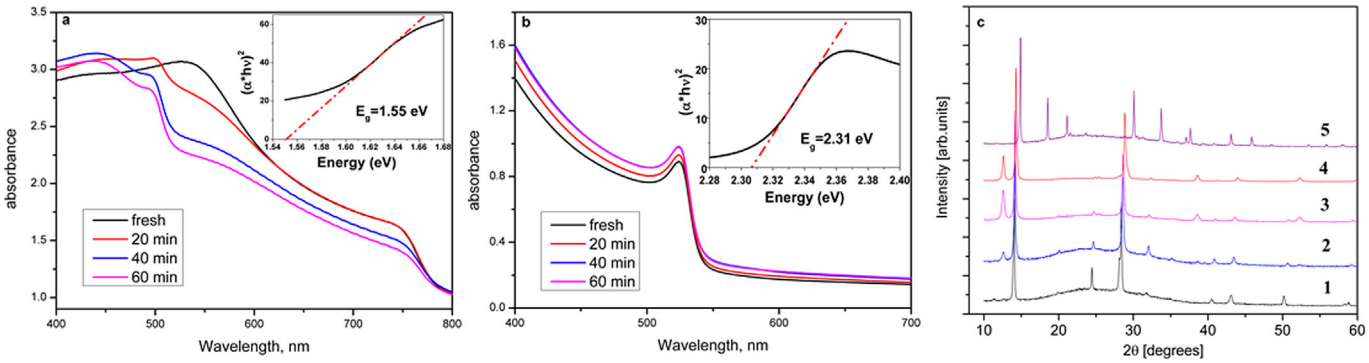

Figure 3. Evolution of UV/Vis light absorbance spectra for (a) $MAPbI_3$ (sample 1) and (b) $MAPbBr_3$ (sample 5) encapsulated films following exposure to concentrated sunlight of 100 suns. The legends indicate the exposure times. The insets show the spectrum of the fresh film near the fundamental absorption edge plotted in Tauc's coordinates.[16] (c) XRD patterns of $MAPb(I_{1-x}Br_x)_3$ films after exposure to concentrated sunlight of 100 suns for 1 h. Increasing sample numbers indicate increasing Br content; for sample details see Table 1.

is within the error estimated for the x values calculated from Vegard's law, resulting from the error in determining the lattice constant (Table 1). Figures 3 and S1 show UV/Vis light absorbance spectra of the various $MAPb(I_{1-x}Br_x)_3$ films. Tauc plots were used to determine the optical band gap (E_g) values (insets in Figure 3).[15,16] The E_g values for $MAPbI_3$ and $MAPbBr_3$ samples are in agreement with previously reported ones (i.e., ~1.58[17] and 2.3 eV,[18] respectively). A gradual increase of the E_g values with increasing Br content is evident (Table 1). We conclude that the mixed halide films have a single phase structure (solid solution) with Br content slightly larger than that expected from the precursor materials, probably owing to the sequential, two-step deposition method (see the Experimental Section for details). The relationship between the halide composition of the precursor solution and the films can be strongly dependent on the technology of the film preparation. Sadhanala et al.[10] and Fedeli et al.[14] confirmed that the ratios of Br to I in their $MAPb(I_{1-x}Br_x)_3$ films are the same as those in the solutions when a stoichiometric precursor composition in a single deposition step was used. However, in other studies,[19] where an excessive amount of MA salts was involved in the film preparation, a discrepancy between actual halide compositions in solid perovskites and initial precursor solutions was reported. In our case, this result can be related to the use of the two-step deposition process where PbI_2 or $PbBr_2$ films were dipped into isopropanol solutions containing MAI and MABr at various ratios.[5] Different reaction rates of the lead halides with MAI versus MABr may control the actual halide composition of the films.

The evolution of light absorption and the corresponding structural modifications in the films following stressing were investigated using UV/Vis absorbance spectroscopy and XRD, respectively. Figure 3a illustrates the evolution of UV/Vis light absorbance spectra for the encapsulated $MAPbI_3$ film owing to its exposure to concentrated sunlight of 100 suns. Concentrated sunlight accelerates stressing via increased light intensity, which can be accompanied by sample heating (see Experimental Section). We have previously shown that the decomposition mechanism of perovskites, such as $MAPbI_3$, is light and thermally enhanced or initiated, while heat alone did not induce decomposition.[7] Following the first 20 min of exposure the absorption decreased in the range of 500–620 nm forming a hump around 500 nm, associated with PbI_2 absorption. With increased exposure time, this decrease expanded to the entire range of the perovskite absorption (500–800 nm) and the hump became more prominent. The overall degradation in absorption of this film was quantified by calculating the absorption degradation state (ADS), that is, the ratio of the number of absorbed solar photons (from the AM 1.5 G spectrum) by the exposed film to that by the fresh sample[7] (for the calculation method see the Supporting Information). This ratio showed a slight gradual decrease with exposure time (by ~2% for 60 min, maximum dose of 100 sun*h, black line in Figure 4a). For this sample, the ratio between the intensity of the XRD peak at 12.4° (related to PbI_2) to that of the peak at 14° (perovskite) was equal to 0.011 before exposure (Figure 1) and 0.020 after exposure for 60 min (Figure 3c), demonstrating the relative increase in PbI_2 content in the film resulting from degradation.

The evolution of light absorption of the mixed halide $MAPb(I_{1-x}Br_x)_3$ films showed similar behavior to that of $MAPbI_3$ but at higher degradation rates (Figures S1 and 4). It is noted that the decrease in the perovskite absorption was partially compensated by the PbI_2 absorption, whose contribution to the PV performance of the cells is negligible. A calculation of the absorption changes in the range of the perovskite's absorption only, without the contribution of PbI_2 absorption (Figure S2) showed similar trends as those presented in Figure 4. It indicates that the degradation of the film absorption at 400–800 nm is dominated by perovskite absorption changes. At the same time, the UV/Vis absorbance spectrum of pure $MAPbBr_3$ did not exhibit any degradation following exposure, but rather a slight improvement in the absorption (Figures 3b and 4). The slight increase in absorption might be explained by enhanced conversion of the $PbBr_2$/MABr precursors to the final $MAPbBr_3$ perovskite in the film. This conversion was not complete in the pristine film, as indicated by the presence of $PbBr_2$ detected by XRD (Figure 1). This effect should be further investigated.

Joint analysis of the light absorbance and XRD data (Figures 1, 3, and S1) suggests that decomposition of the perovskite via crystallization of PbI_2 occurs during exposure of $MAPbI_3$ film and mixed halide $MAPb(I_{1-x}Br_x)_3$ films, in accord-

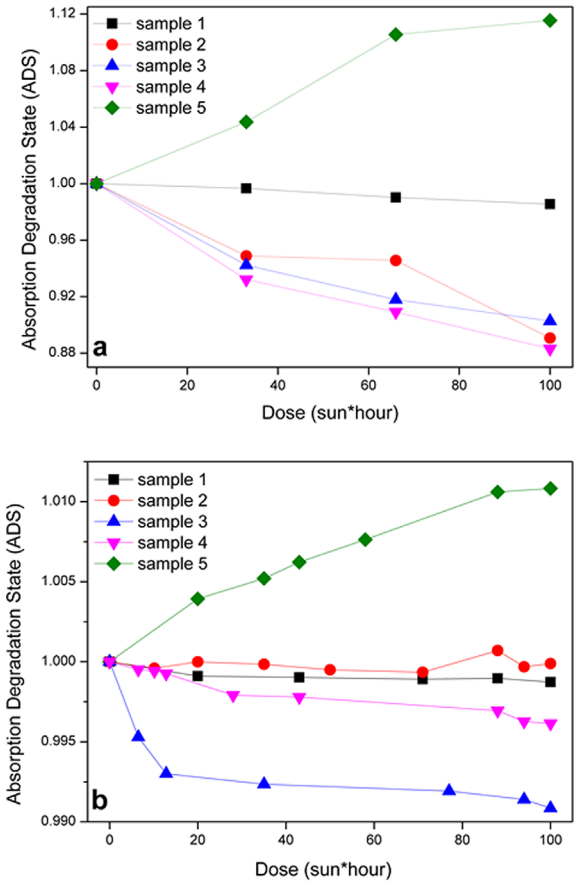

Figure 4. ADS of $MAPb(I_{1-x}Br_x)_3$ films as a function of the exposure dose under illumination of (a) 100 suns and (b) outdoor solar exposure. Increasing sample numbers indicate increasing Br content; for sample details see Table 1.

ance with our recent results.[7] Decomposition of $MAPbI_3$ to PbI_2 and MAI was previously suggested as the result of photolysis, with further dissociation of MAI to CH_3NH_2, I_2, and other small molecules (e.g., H, HI, H_2O).[20–22] PbI_2 crystallization was directly confirmed herein by XRD measurements (Figure 3c). The observed shift of the XRD perovskite-related peaks towards higher 2θ values following exposure (Figure 2) indicated an increased Br content in the remaining perovskites following PbI_2 release. The lack of splitting of these perovskite-related XRD peak suggests no phase separation to the $MAPbI_3$ and $MAPbBr_3$ perovskites. Fourier transformed infrared spectroscopy (FTIR) measurements showed a decrease in organic (carbon- and nitrogen- related) groups' absorption, with no alternative peaks rising (Figure S3), indicating their elimination from the solid film. Electron paramagnetic resonance spectroscopy of our perovskite samples illuminated by 100 suns in a closed ampoule showed the involvement of MAI dissociation in the degradation process (to be published elsewhere). We therefore suggest a photolysis decomposition of the mixed halide perovskite to MAI, PbI_2, and a Br-richer mixed halide perovskite as a possible first step, which is followed by further MAI decomposition into volatile species and I_2.[20–22] Small quantities of PbI_2 were previously suggested to be beneficial for $MAPbI_3$-based cell performance, by passivating surface defects and reducing recombination at the perovskite/TiO_2 interface.[23–25] However, the presence of PbI_2 was found to accelerate $MAPbI_3$ photo-degradation,[26] and it may have an autocatalytic effect also on mixed-halide perovskite degradation.

To establish the relevance of accelerated testing by concentrated sunlight to standard operational conditions of PV cells, the evolution of UV/Vis light absorbance spectra of $MAPb(I_{1-x}Br_x)_3$ films was recorded during their exposure to natural outdoor sunlight. We note that the degradation occurred only under illumination and no degradation was recorded after overnight shelf storage. Figure 4b shows the ADS evolution during exposure to 100 sun*h. This accumulated dose is equivalent to the dose that samples experienced during 1 h under 100 suns. Though the observed ADS variations are at least an order of magnitude smaller than those under the same dose of concentrated sunlight (i. e., the acceleration ratio in the concentrated sunlight experiments was larger than 100, owing to the combined effect of increased light intensity and temperature),[7] the results showed the same trend of ADS evolution. Indeed, $MAPbBr_3$ film exhibited improved ADS following exposure, while increased Br content in the films accelerated the absorption degradation.

We conclude that, though $MAPbBr_3$ is the most stable composition, increased Br content in the mixed halide perovskite films resulted in accelerating their photochemical degradation. The relative changes in absorption are shown by the blue curve in Figure 5 showing the normalized difference in absorption following degradation (1−ADS) as a function of Br content in the film (x) calculated using the XRD analysis (Table 1). Absorption degradation was found to correlate with increased full width at half maximum (FWHM) of the XRD peaks for mixed halide perovskites compared to $MAPbI_3$ and $MAPbBr_3$ (Figure 5 and Table 1). The FWHM of XRD peaks is inversely related to the crystal coherence length; therefore, the observed FWHM increase for $MAPb(I_{1-x}Br_x)_3$ indicates that the mixed halide compounds contain more structural defects and/or grain boundaries in comparison with pure halide perovskites. The decreased grain sizes in the mixed halide films (in comparison with those in $MAPbI_3$ and $MAPbBr_3$ samples) have been

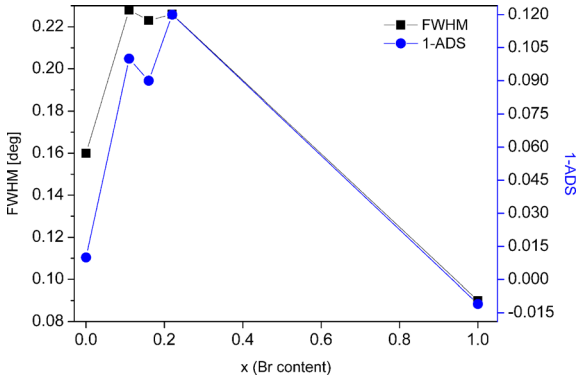

Figure 5. Correlation between the FWHM of the XRD peaks for fresh $MAPb(I_{1-x}Br_x)_3$ films and the degree of their degradation indicated by (1−ADS), after their exposure to concentrated sunlight of 100 suns for 1 h. XRD peaks used for FWHM analysis are indicted in Table 1. The x values were determined from XRD analysis.

confirmed by scanning electron microscopy (Figure S4). A similar behavior of the FWHM of the XRD peaks was observed in $MAPb(I_{1-x}Br_x)_3$ films by Fedeli et al.,[14] who also observed correlated changes in the Urbach energy, which may be related to structural disorder. Furthermore, both Fedeli et al.[14] and Sadhanala et al.[10] found that changes in the FWHM of PL peaks were correlated with the Urbach energy variations, that is, the band-to-band PL peak became narrower when the Urbach energy was smaller (less structural disorder) at low and high x values, and vice versa at intermediate x values. The larger PL peak FWHM and Urbach energies for films with intermediate x, compared with films with higher I or Br content, correlated with shorter lifetimes observed in transient PL.[10] This further supports our assumption of larger structural disorder in mixed halide perovskite compositions. A similar behavior of the FWHM of the XRD peaks as a function of composition was previously observed also for $MASn(I_{1-x}Br_x)_3$ solid solutions,[27] and no crystalline solid solutions could be formed in $FAPb(I_{1-x}Br_x)_3$ (FA = formamidinium) for $0.3 < x < 0.5$, indicating reduced crystal quality in these perovskite mixed halide solutions.[28]

Both the smaller crystal coherence length and the enhanced decomposition rate of the mixed perovskite films can be explained by the presence of two different halide ions with different sizes occupying six coordinating sites around the central Pb^{II} cation. This may result in the distortion of the skeletal octahedral structure of $[PbI_6]^{4-}$ and a corresponding strain amplification in the pseudo-cubic geometry of the $MAPb(I_{1-x}Br_x)_3$ solid solutions. The correlation between the decreased crystal coherence length and the increased degradation rate suggests that the perovskite photo-induced decomposition might be associated with increased structural defect concentration rather than the halide composition. Indeed, grain boundaries and defects are thought to play a significant role in initiating photochemical degradation in perovskites.[29,30] It was recently shown that large grained films of $MAPbI_3$ with enhanced crystallinity demonstrated improved ambient stability,[31] and that post-deposition $MAPbI_3$ crystal crosslinking enhanced the device stability.[30] Furthermore, our results may suggest the crystal coherence length as an indicator for the relative photolysis degradation rate, and that perovskites with a smaller structural defect concentration should be more stable to photolysis.

In summary, encapsulated films of mixed halide perovskites with a range of $MAPb(I_{1-x}Br_x)_3$ compositions were prepared, and their composition and stability were characterized. The films were found to have a single phase crystalline structure with Br content slightly larger than that expected from the precursor materials. Exposure to concentrated sunlight of 100 suns and to outdoor 1 sun did not result in degradation of the $MAPbBr_3$ films, while $MAPbI_3$ and mixed halide $MAPb(I_{1-x}Br_x)_3$ films degraded yielding crystallization of PbI_2 and the corresponding degradation of light absorption. Increased Br content accelerated this process. We relate this finding with an observed increase in the FWHM of the mixed halide perovskite XRD peaks (i.e., decreased crystal coherence length). This suggests that the perovskite degradation might be associated with increased defect concentration rather than the halide composition, and that perovskites with a smaller defect concentration should be more stable to photolysis. The role of defects and grain boundaries in the photochemical degradation of perovskite PV materials should be a topic of further research.

Experimental Section

Synthesis of $MAPb(I_{1-x}Br_x)_3$ perovskites and film preparation: MAI and MABr were synthesized as described earlier,[5] by reacting 30 mL of CH_3NH_2 (40% in CH_3OH, TCI) and 32.3 mL of HI (57 wt% in H_2O, Aldrich) or 23.32 mL of HBr (48wt% in H_2O, Aldrich) in a 250 mL round bottom flask at 0 °C for 2 h while stirring. The precipitate was recovered by putting the solution in a rotatory evaporator and carefully removing the solvents at 50 °C for 1 h. The yellowish raw product of MAI or MABr was washed thrice in diethyl ether by stirring the mixture for 30 min. After filtration, the solid was collected and dried at 60 °C in a vacuum oven for 24 h. The films of $MAPb(I_{1-x}Br_x)_3$ were prepared using the sequential deposition method.[32] A 1 M solution of PbI_2 (Sigma Aldrich) or $PbBr_2$ (Sigma Aldrich) in dimethylformamide (DMF, Sigma Aldrich) was spin-coated onto a glass substrate (in O_2- and H_2O-free nitrogen atmosphere) at 6000 rpm for 5 s, followed by annealing for 5 min at 90 °C on a hot plate. Then PbI_2 films were dipped for 30 s into one of the following solutions in 10 mL isopropanol (Sigma–Aldrich): 0.100 g MAI (sample 1), 0.067 g MAI + 0.0235 g MABr (sample 2), 0.050 g MAI + 0.0352 g MABr (sample 3), or 0.033 g MAI + 0.047 g MABr (sample 4). We note that the mixed halide compositions studied herein are limited to maximum Br content of $x \approx 0.4$. $PbBr_2$ films were dipped in a solution of 0.070 g MABr in 10 mL isopropanol (sample 5). After dipping, samples were annealed for 30 min at 90 °C on a hot plate. The Br content calculated from the precursor materials took into account the halide contribution from the inorganic and the organic precursors, divided by 3; for example, films made from PbI_2 (contributing 2 I atoms) and MAI/MABr 2:1 (contributing 0.66 I and 0.33 Br atoms) were expected to yield the perovskite composition of $MAPbI_{2+0.66}Br_{0.33}$ (i.e., $x = 0.33/3 = 0.11$). Encapsulation of these films was done inside a glovebox using a DuPont™ Surlyn® film as a spacer and sticker for the upper glass by melting it using a welding pen. The current study was aimed at studying the perovskite material stability, hence it was not measured in a cell configuration where other failure mechanisms (e.g., contacts, charge selective layers) may mask the perovskite behavior. Similarly, a mesoporous TiO_2 substrate may introduce additional degradation mechanism induced by excitation under UV illumination and release of oxygen radicals,[33,34] hence it was avoided.

Film exposure to concentrated sunlight: Sunlight collected and concentrated outdoors was focused into a transmissive optical fiber and delivered indoors onto the sample (Figure S5 a).[35,36] A 2.5 cm long, 0.25 cm^2 square cross-section kaleidoscope placed between the distal fiber tip and the sample was used to achieve flux uniformity (Figure S5 b).[36] Sunlight exposure was performed at Sede Boqer (Lat. 30.8°N, Lon. 34.8°E, Alt. 475 m) during clear-sky periods around 12:00 pm, where the solar spectrum was found to be very close to the standard AM 1.5 G solar spectrum.[37] The spectrum of light delivered to the sample was also close to the AM 1.5 standard.[35] The concentration of incident sunlight on the sample was measured using a spectrally blind pyranometer (thermopile) of 5% accuracy. During the exposure, the samples were thermally bonded to the top of a thermoelectric temperature controlled plate, which was set to 25 °C. The temperature at the sample/thermoelectric plate interface was measured with a T-type thermocou-

ple connected to the sample using silver paste. The sample temperature during illumination was about 45–55 °C.

Film exposure to outdoor sunlight. Solar exposure of the samples was performed during the day in July–August 2015 with permanent monitoring of the intensity of incident sunlight and the sample temperature, while during the night the films were kept in the dark in a glovebox. Global intensity of incident sunlight was measured with a calibrated thermopile pyranometer (Eppley PSP). The sample and the pyranometer were mounted on a fixed angle stand (30° to horizontal, see for example Figure 6c in Ref. [38]). The samples experienced ambient temperatures (25–35 °C) measured by thermocouples.

Optical and crystallographic characterization. The UV/Vis absorbance spectra of the films before and after exposure were recorded in direct transmission mode using a Cary 5000 UV–vis–NIR spectrophotometer (Agilent technologies). To verify that diffuse scattering was not responsible for the observed changes in the measured absorbance, the diffuse scattering intensity spectra were measured and were found to be almost entirely independent of the sample's light exposure (Figure S6). The absorbance is defined as $A = \varepsilon c l$, where ε is the attenuation coefficient, c is the concentration of the absorbing species in the film, and l is the film thickness. Hence changes in A reflect the changes in the concentration of the absorbing species in the film, c. XRD data were collected with Panalytical Empyrean Powder Diffractometer equipped with position sensitive X'Celerator detector using CuKα radiation ($\lambda = 1.5405$ Å) and operated at 40 kV and 30 mA.

Acknowledgements

R.K.M., L.C., L.E., E.A.K., and I.V-F. are members of the European Commission's StableNextSol COST Action MP1307. The research was funded by the in part by Israel's Ministry of National Infrastructures, Water and Energy Resources (grant no. 0399202/215-11-037) and by the Adelis Foundation. L.E. thanks the German Israel Foundation for its financial support for Young Researchers. R.K.M. is thankful to BGU's Blaustein Center for Scientific Cooperation for a postdoctoral research fellowship. L.C. is thankful to ENEA (Ente Nazionale Energia e Ambiente) and the Italian Ministry of Foreign Affairs for a visitor fellowship.

Keywords: mixed halide perovskites · organic-inorganic hybrid composites · photolysis · photovoltaics · stability

[1] W. S. Yang, J. H. Noh, N. J. Jeon, Y. C. Kim, S. Ryu, J. Seo, S. I. Seok, *Science* **2015**, *348*, 1234–1237.
[2] D. B. Mitzi, C. A. Feild, Z. Schlesinger, R. B. Laibowitz, *J. Solid State Chem.* **1995**, *114*, 159–163.
[3] E. Mosconi, A. Amat, M. K. Nazeeruddin, M. Grätzel, F. De Angelis, *J. Phys. Chem. C* **2013**, *117*, 13902–13913.
[4] J. H. Noh, S. H. Im, J. H. Heo, T. N. Mandal, S. I. Seok, *Nano Lett.* **2013**, *13*, 1764–1769.
[5] S. Aharon, B. E. Cohen, L. Etgar, *J. Phys. Chem. C* **2014**, *118*, 17160–17165.
[6] I. Visoly-Fisher, A. Mescheloff, M. Gabay, C. Bounioux, L. Zeiri, M. Sansotera, A. Goryachev, A. Braun, Y. Galagan, E. Katz, *Solar Energy Mater. Solar Cells* **2015**, *134*, 99–107.
[7] R. K. Misra, S. Aharon, B. Li, D. Mogilyansky, I. Visoly-Fisher, L. Etgar, E. A. Katz, *J. Phys. Chem. Lett.* **2015**, *6*, 326–330.
[8] Y. Rong, L. Liu, A. Mei, X. Li, H. Han, *Adv. Energy Mater.* **2015**, n/a-n/a.
[9] E. T. Hoke, D. J. Slotcavage, E. R. Dohner, A. R. Bowring, H. I. Karunadasa, M. D. McGehee, *Chem. Sci.* **2015**, *6*, 613–617.
[10] A. Sadhanala, F. Deschler, T. H. Thomas, S. E. Dutton, K. C. Goedel, F. C. Hanusch, M. L. Lai, U. Steiner, T. Bein, P. Docampo, D. Cahen, R. H. Friend, *J. Phys. Chem. Lett.* **2014**, *5*, 2501–2505.
[11] A. Poglitsch, D. Weber, *J. Chem. Phys.* **1987**, *87*, 6373–6378.
[12] A. Kojima, K. Teshima, Y. Shirai, T. Miyasaka, *J. Am. Chem. Soc.* **2009**, *131*, 6050–6051.
[13] L. Vegard, *Z. Phys.* **1921**, *5*, 17–26.
[14] P. Fedeli, F. Gazza, D. Calestani, P. Ferro, T. Besagni, A. Zappettini, G. Calestani, E. Marchi, P. Ceroni, R. Mosca, *J. Phys. Chem. C* **2015**, *119*, 21304–21313.
[15] G. E. Eperon, S. D. Stranks, C. Menelaou, M. B. Johnston, L. M. Herz, H. J. Snaith, *Energy Environ. Sci.* **2014**, *7*, 982–988.
[16] J. Tauc, R. Grigorovici, A. Vancu, *Phys. Status Solidi B* **1966**, *15*, 627–637.
[17] X. Xu, C. Randorn, P. Efstathiou, J. T. S. Irvine, *Nat. Mater.* **2012**, *11*, 595–598.
[18] S. T. Ha, X. Liu, Q. Zhang, D. Giovanni, T. C. Sum, Q. Xiong, *Adv. Opt. Mater.* **2014**, *2*, 838–844.
[19] S. A. Kulkarni, T. Baikie, P. P. Boix, N. Yantara, N. Mathews, S. Mhaisalkar, *J. Mater. Chem. A* **2014**, *2*, 9221–9225.
[20] G. Niu, W. Li, F. Meng, L. Wang, H. Dong, Y. Qiu, *J. Mater. Chem. A* **2014**, *2*, 705–710.
[21] J. M. Frost, K. T. Butler, F. Brivio, C. H. Hendon, M. van Schilfgaarde, A. Walsh, *Nano Lett.* **2014**, *14*, 2584–2590.
[22] L. A. Frolova, N. N. Dremova, P. A. Troshin, *Chem. Commun.* **2015**, *51*, 14917–14920.
[23] D. H. Cao, C. C. Stoumpos, C. D. Malliakas, M. J. Katz, O. K. Farha, J. T. Hupp, M. G. Kanatzidis, *APL Mater.* **2014**, *2*, 091101.
[24] Q. Chen, H. Zhou, T.-B. Song, S. Luo, Z. Hong, H.-S. Duan, L. Dou, Y. Liu, Y. Yang, *Nano Lett.* **2014**, *14*, 4158–4163.
[25] L. Wang, C. McCleese, A. Kovalsky, Y. Zhao, C. Burda, *J. Am. Chem. Soc.* **2014**, *136*, 12205–12208.
[26] F. Liu, Q. Dong, M. K. Wong, A. B. Djurišić, A. Ng, Z. Ren, Q. Shen, C. Surya, W. K. Chan, J. Wang, A. M. C. Ng, C. Liao, H. Li, K. Shih, C. Wei, H. Su, J. Dai, *Adv. Energy Mater.* **2016**, *6*, 1502206.
[27] K. Yamada, K. Nakada, Y. Takeuchi, K. Nawa, Y. Yamane, *Bull. Chem. Soc. Jpn.* **2011**, *84*, 926–932.
[28] G. E. Eperon, S. D. Stranks, C. Menelaou, M. B. Johnston, L. M. Herz, H. J. Snaith, *Energy Environ. Sci.* **2014**, *7*, 982–988.
[29] Y. Shao, Z. Xiao, C. Bi, Y. Yuan, J. Huang, *Nat. Commun.* **2014**, *5*, 5784.
[30] X. Li, M. Ibrahim Dar, C. Yi, J. Luo, M. Tschumi, S. M. Zakeeruddin, M. K. Nazeeruddin, H. Han, M. Grätzel, *Nat. Chem.* **2015**, *7*, 703–711.
[31] H.-J. Yen, P.-W. Liang, C.-C. Chueh, Z. Yang, A. K. Y. Jen, H.-L. Wang, *ACS Appl. Mater. Interfaces* **2016**, *8*, 14513–14520.
[32] C. Bi, Y. Yuan, Y. Fang, J. Huang, *Adv. Energy Mater.* **2015**, *5*, 1401616.
[33] T. A. Berhe, W.-N. Su, C.-H. Chen, C.-J. Pan, J.-H. Cheng, H.-M. Chen, M.-C. Tsai, L.-Y. Chen, A. A. Dubale, B.-J. Hwang, *Energy Environ. Sci.* **2016**, *9*, 323–356.
[34] S. K. Pathak, A. Abate, T. Leijtens, D. J. Hollman, J. Teuscher, L. Pazos, P. Docampo, U. Steiner, H. J. Snaith, *Adv. Energy Mater.* **2014**, *4*, 1301667.
[35] J. M. Gordon, E. A. Katz, D. Feuermann, M. Huleihil, *Appl. Phys. Lett.* **2004**, *84*, 3642–3644.
[36] E. A. Katz, J. M. Gordon, W. Tassew, D. Feuermann, *J. Appl. Phys.* **2006**, *100*, 044514.
[37] D. Berman, D. Faiman, *Sol. Energy Mater. Sol. Cells* **1997**, *45*, 401–412.
[38] J. Kettle, N. Bristow, D. T. Gethin, Z. Tehrani, O. Moudam, B. Li, E. A. Katz, G. A. dos Reis Benatto, F. C. Krebs, *Solar Energy Mater. Sol. Cells* **2016**, *144*, 481–487.

Received: May 22, 2016
Revised: July 11, 2016
Published online on ■■ ■■, 0000

COMMUNICATIONS

To be or not to be (efficient *and* stable): Photochemical stability studies of $MAPb(I_{1-x}Br_x)_3$ (MA = methylammonium) photovoltaic materials show that mixed halide compositions are less stable than pure halide ones. We postulate that these solid solutions contain internal stresses and structural defects, which might be responsible for their accelerated degradation.

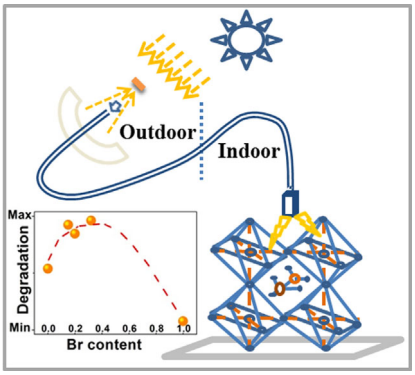

R. K. Misra, L. Ciammaruchi, S. Aharon, D. Mogilyansky, L. Etgar, I. Visoly-Fisher, E. A. Katz**

■■ – ■■

Effect of Halide Composition on the Photochemical Stability of Perovskite Photovoltaic Materials

These are not the final page numbers! ↗↗